JOURNAL OF GEOPHYSICAL RESEARCH, VOL. 103, NO. D2, PAGES 1747–1758, JANUARY 27, 1998

A study of the low-frequency inertio-gravity waves observed during the Pyrénées Experiment

C. M. Scavuzzo and M. A. Lamfri
Facultad de Matematica, Astronomia y Fisica, Universidad Nacional de Cordoba, Cordoba, Argentina

H. Teitelbaum and F. Lott
Laboratoire de Météorologie Dynamique, Ecole Normale Supérieure, Paris, France

Abstract. The purpose of this paper is to analyze and interpret the onset of some well-characterized transient inertio-gravity waves, observed during the PYREX (Pyrénées Experiment) campaign. The data used are the high-resolution soundings, launched every 6 hours on both sides of the ridge. In agreement with other observations made during the field campaign, certain among those soundings often show steady mountain waves. It appears that those waves are often transients and are followed by well-characterized inertio-gravity waves, propagating upward and downward from the level where the initial mountain waves are large. To interpret those observations, it is suggested that the observed inertio gravity waves result from the geostrophic adjustment of the large-scale flow that follows the transit and eventually the breaking of the main mountain wave. This hypothesis is supported by an analytical calculation of inertio-gravity waves emission from a momentum deposit that lasts a finite time. The spatial extent of this forcing are also finite, and its maximum amplitude is a fraction of the measured mountain drag.

1. Introduction

Sources of gravity waves in the atmosphere have received much attention because they are known to influence local meteorology as well as the large-scale atmospheric circulation. Important tropospheric sources are believed to include topography [*Queney,* 1947; *Smith,* 1979; *Palmer et al.,* 1986; *Lott and Teitelbaum,* 1993], convective and frontal activities [*Bretherton and Smolarkiewitcz,* 1989; *Shutts and Gray,* 1994], wind shear [*Lalas and Einaudi,* 1976; *Rosenthal and Lindzen,* 1983; *Fritts,* 1982; *Lott et al.,* 1992] and geostrophic adjustment [*Rossby,* 1937; *Blumen,* 1972; *Fritts and Luo,* 1992]. In the later case, many studies examined geostrophic adjustment in an idealized way, as a linear relaxation from an initial imbalance of momentum or mass toward a balanced state, fully described by the potential vorticity distribution. These studies assume that the adjustment is rapid compared to the evolution of potential vorticity, as it is the case when the momentum forcing due to the breaking mountain waves lasts long compared to the advective timescale. In this case, and for three-dimensional obstacles, the large-scale flow response is a wake entirely described by potential vorticity streamers located downstream of the mountain [*Schär and Durran,* 1996]. Nevertheless, examples of geostrophic adjustments can also occur for mountain flows. For example, [*Mattocks and Bleck,* 1986] have suggested that geostrophic adjustment occurs during the process of lee cyclogenesis so that inertio-gravity waves are often large near mountains. Another possibility that has not been yet considered is that the onset of wave breaking at a given high altitude is very transient. In this case the large-scale flow response should essentially be made of inertio gravity waves, a balanced state being too long to be reached. For this purpose the PYREX campaign provide a rather coherent database [*Bougeault et al.,* 1993]. Among many different measurements, numerous high-resolution soundings were launched every 6 hours during the PYREX PIO (periods of intense observation), and they provide accurate vertical sections of the atmosphere. The object of this paper is to analyze and to understand the wave field that can be observed in these soundings.

In section 2 the high-resolution soundings launched near the ridge of the Pyrénées during the PYREX campaign are analyzed. They show that under certain atmospheric configurations, rather coherent inertio-gravity waves can be observed near the mountain ridge. A possible mechanism for their generation is proposed in section 3. It suggests that the inertial waves result from the geostrophic adjustment of the large-scale flow after the transit of the main mountain waves. The realism of this mechanism is supported by the fact that the observed pressure drag varies a lot over short time scales.

Paper number 97JD02308.
0148-0227/98/97JD-02308$09.00

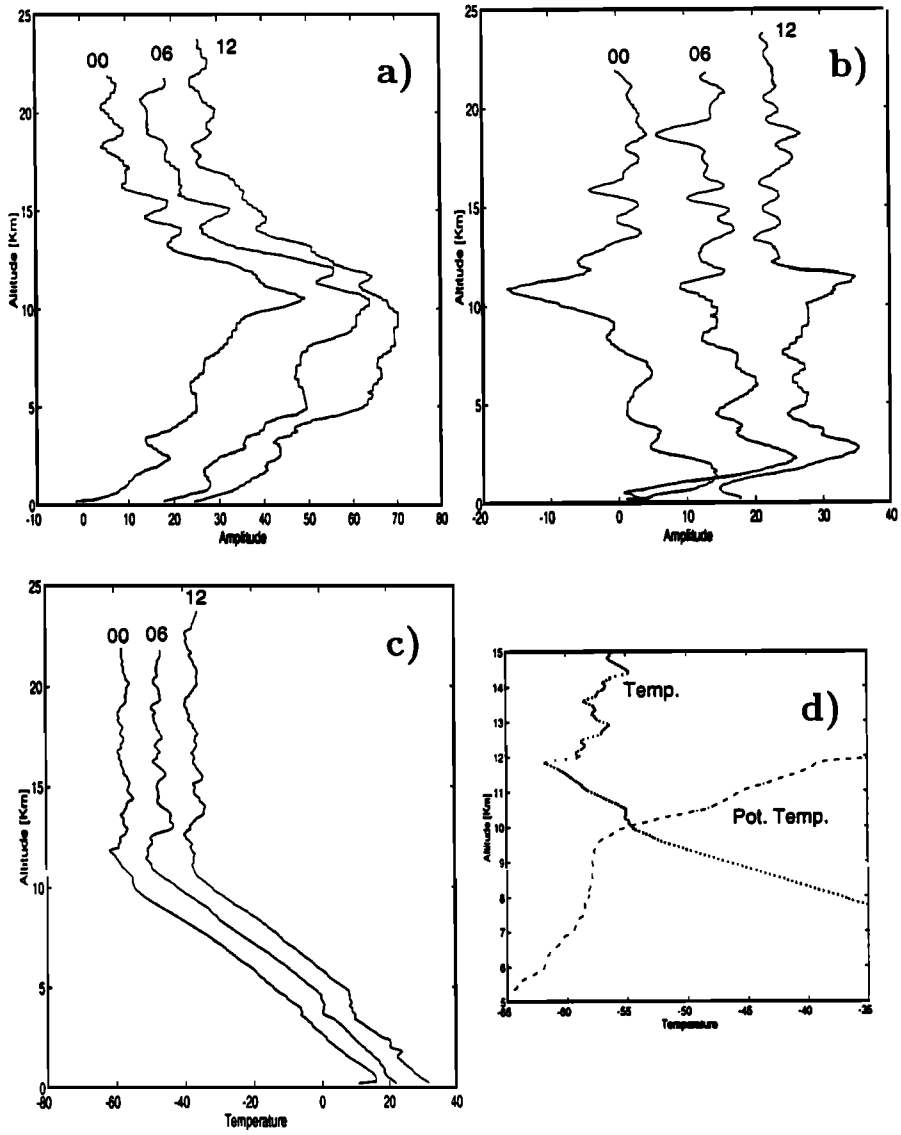

Figure 1. Pau soundings, unfiltered data of October 26, 1990 at 0, 6 and 12 UT. (a) Zonal wind, (b) meridional wind, (c) temperature and (d) temperature and potential temperature at 0 UT.

The corresponding forcing on the large-scale flow varies accordingly, so that there is little chance for its response to be always balanced. The Appendix presents the filters that have been used to extract the wave signal from the soundings.

2. Observations

The data used in this study were obtained from soundings launched from Pau (43°23'N; 0°25'W) and Pampelone (47°45'N; 1°38'W). In most cases the soundings launched from one of these two stations, which is located downstream of the Pyrénées are analyzed. Indeed, the downstream soundings often show larger waves than the upstream soundings, which make their analysis more tractable. Nevertheless, this difference is not sharp, and examples where upstream and downstream soundings are compared are also given. Each radiosounding gives high-resolution ($\delta z \approx 50$m) profiles of temperature, humidity and altitude. These soundings also give horizontal wind at the same altitude after a smoothing applied routinely to suppress the noise due to the inaccuracy of the positionning of the balloons by the Loran-C (or the Omega) system used. This operational smoothing is a kind of moving average whose buffer length varies with altitude; during PYREX it was below 1200m (P. Bessemoulin, private communication, 1997). For these data, the processing of wind and temperature profiles is made in two steps. First, a cubic spline is applied that transforms the irregularly spaced profile into a regular one with resolution $\delta z = 50$m. Then, in order to isolate the wave pattern, a band-pass filter which spans vertical wavelength typically ranging from 2 to 6 km is applied. The filter used

is non recursive, and to avoid Gibbs effects, a Kaiser window is used [*Hamming,* 1983] (see Appendix for details).

The first analysis, concerns a sequence of three soundings, launched from Pau at 0, 6 and 12 UT October 26. The Figures 1a-1c, display the unfiltered sequences of zonal wind, meridional wind and temperature, respectively. In both profiles of u and v, a pronounced narrow peak is observed just above 10 km at 0 UT. Thermodynamics variables, like temperature and potential temperature (Figure 1d), also show pronounced anomalies at the same place. At this height, the temperature is colder than anywhere else, which in absence of a corresponding minima of the potential temperature suggests that an upward distortion of the tropopause has occurred, and the temperature minima is related to a dilatation (adiabatic cooling). Furthermore, other observations confirm that this anomaly can be related to gravity waves. For instance, the ground observations at Beggar and Guinarte (i.e., rather close from Pau) ([*Champeaux and Peris,* 1991] pp. 146-147) shows abrupt increase of temperature and decrease of humidity, between October 25 at 22 UT and October 26 at 4 UT that are clear signatures of a Foehn. The fact that mountain waves forcing at the ground were large during a short period of time this day is further indicated by the pressure drag records [*Bessemoulin et al.,*1993] which show a pronounced minimum that lasts less than a day and descends below -6 Pa. On the same figure, the potential temperature profile shows that near 10 km, the potential temperature gradient is near zero, suggesting that the mountain waves at this level are close from breaking. This last interpretation should nevertheless be considered with great care. Indeed, the observation of isentropic layers in a balloon ascent does not necessarily mean that the corresponding atmospheric layer is isentropic in the vertical direction. This follows that the balloon trajectory is inclined in the direction of the wind and can locally become tangent to a constant isentropic surface, when the former is distorted by the presence of the main mountain waves. Accordingly, an individual sounding can overstate (or understate) the appearance of mixed layers. Furthermore, one of the results of the PYREX campaign was that the onset of breaking waves at high levels was not systematic: in a case of strong low-level wind (October 15, 1990, PIO3) that has been very much documented and selected as an exercise in the COMPARE project, no breaking waves were observed by the airplanes flight aloft. Wave breaking is also absent from most of the three-dimensional numerical simulations that were made in the course of the COMPARE exercise for the same date (in agreement with the simulations presented by [*Georgelin et al.,* 1994]). On the other hand, the analysis of the soundings for this particular date shows adiabatic lapse rates, proving that the onset of adiabatic lapse rates in the soundings does not necessarily follow wave breaking. With this limitation in mind, it remains that the observation of adiabatic lapse rates in the sounding, together with the observation of strong anomalies in the wind field indicate at least that the main mountain waves are large around z=10 km.

Figures 2a-2c show the perturbations fields of the horizontal velocity component, u and v, that are extracted from the soundings shown on the Figure 1 at the same times, 0, 6 and 12 UT respectively. At 0 UT, the Figure 2a shows that around 10 km the wind components are in phase opposition. This indicates that the disturbance there is of high intrinsic frequency, as can be expected for mountain waves. Here it should be noticed that the vertical wavelength of the disturbance shown on Figure 2a (around 4 km at z=10 km) is an apparent one. It is shorter than the one that could be expected for mountain waves because the mountain waves tilt upstream in the direction of the mean wind, while the balloon trajectory tilts in the other direction as it is transported by the flow. Consequently, the balloon intersects two equivalent phase surfaces after a vertical displacement shorter than the actual vertical wavelength. At 6 UT, above 10 km, the wind components are roughly a quarter of cycle out of phase, indicating low-frequency gravity waves. It is noteworthy that the vertical wavelength is smaller in the stratosphere than in the troposphere, features which naturally follow that the stratification (i.e., change of the buoyancy frequency) is very different in these two regions of the atmosphere. The most striking aspect is the variation of the angle of rotation of the horizontal velocity vector shown in Figures 2d-2f. At 6 UT there is a change in the sense of rotation at the level where the mountain waves were large 6 hours before: the rotation is anticlockwise below and clockwise above. These rotations in the northern hemisphere indicate upward and downward wave energy propagation, issued from the level where the mountain waves break. We can remark that these characteristic rotations are not as clear at 0 and 12 UT. If we admit that the mountain waves break at 0 UT we can expect that the inertial wave generated by the geostrophic adjustment takes some time to appear and then dissipates or propagate away, explaining this temporal evolution.

On November 29 the synoptic wind (not shown) is from the north, so mountain waves are expected on the south of the Pyrénées. Figures 3a-3b display the perturbations of the horizontal wind components at 6 and 12 UT, respectively, for soundings launched from Pampelone. On this figure also is observed at 6 UT a strong wind perturbation at 7.5 km for which the zonal and meridional components are in phase. The same structure, at the same level, but with a smaller amplitude is seen at 12 UT. This shows that we are in the presence of rather steady mountain waves. Furthermore, potential temperature profile at 6 UT is close to adiabaticity, indicating that at the time where the amplitude of this disturbance is the largest, it is also close from breaking. Once again, 6 hours later, above and below 7.5 km,

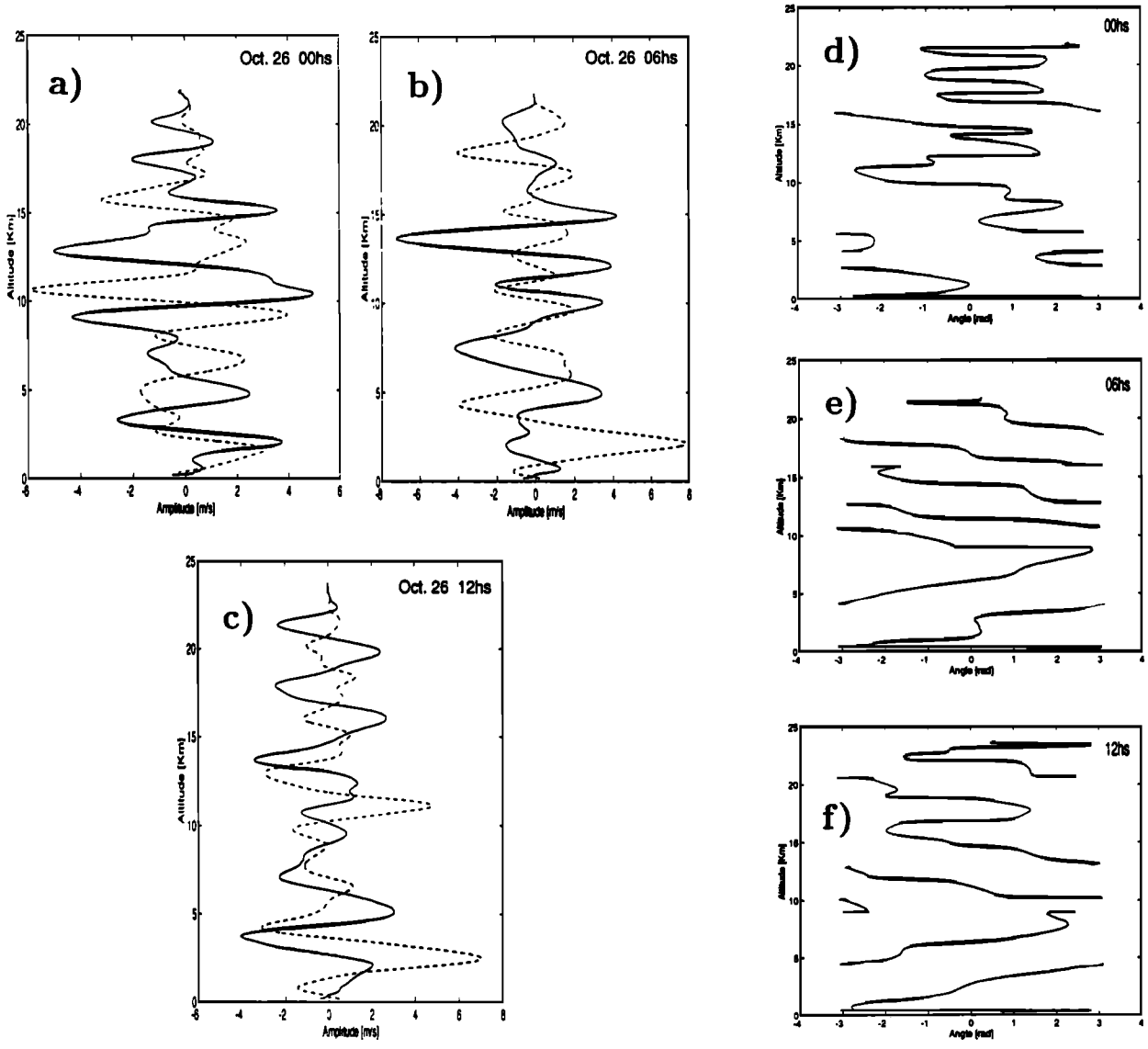

Figure 2. Pau soundings, filtered winds of October 26, 1990. (a-c) Zonal wind (solid), meridional wind (dashed), (e-g) Angle of the wind.

waves are observed, for which the horizontal and meridional wind are roughly a quarter of cycle out of phase (Figure 3f), the rotation being clockwize above 7.5 km and anticlockwise below. Here again it is important to note that these inertio gravity waves are not observed at 0 and 6 UT, suggesting again that they follow the large mountain waves occurring at 6 UT.

Another case whose particularity is that the mountain wave is found at lower levels than the previous ones is shown in Figure 4. The wind profiles have been obtained over Pampelone on November 4 at 18 UT and November 5 at 0 UT. On the first sounding one sees an important perturbation of the horizontal wind around 4 km. Around this altitude the wind components remain in phase, indicating again that they result from rather high intrinsic frequency mountain waves. This perturbation is no longer present 6 hours later. At this time and above 5 km there is a small-amplitude perturbation of the wind whose components are roughly a quarter of cycle out of phase. The phase lag between the two components of the horizontal wind shows again that low frequency waves propagate upward above z=4 km.

In the preceding analysis only downstream soundings were analyzed. Nevertheless, this choice was rather made for convenience, essentially because downstream soundings more often show the temporal evolution from the main steady mountain waves to the inertio-gravity waves described before than the upstream soundings do. Energy spectra also show systematically that the downstream soundings located close to the ridge present stronger wave activity than the others (i.e., those located upstream or far from the ridge). Although this could reinforce the impression that inertio-gravity waves are the largest there, it is to be emphasized that it is

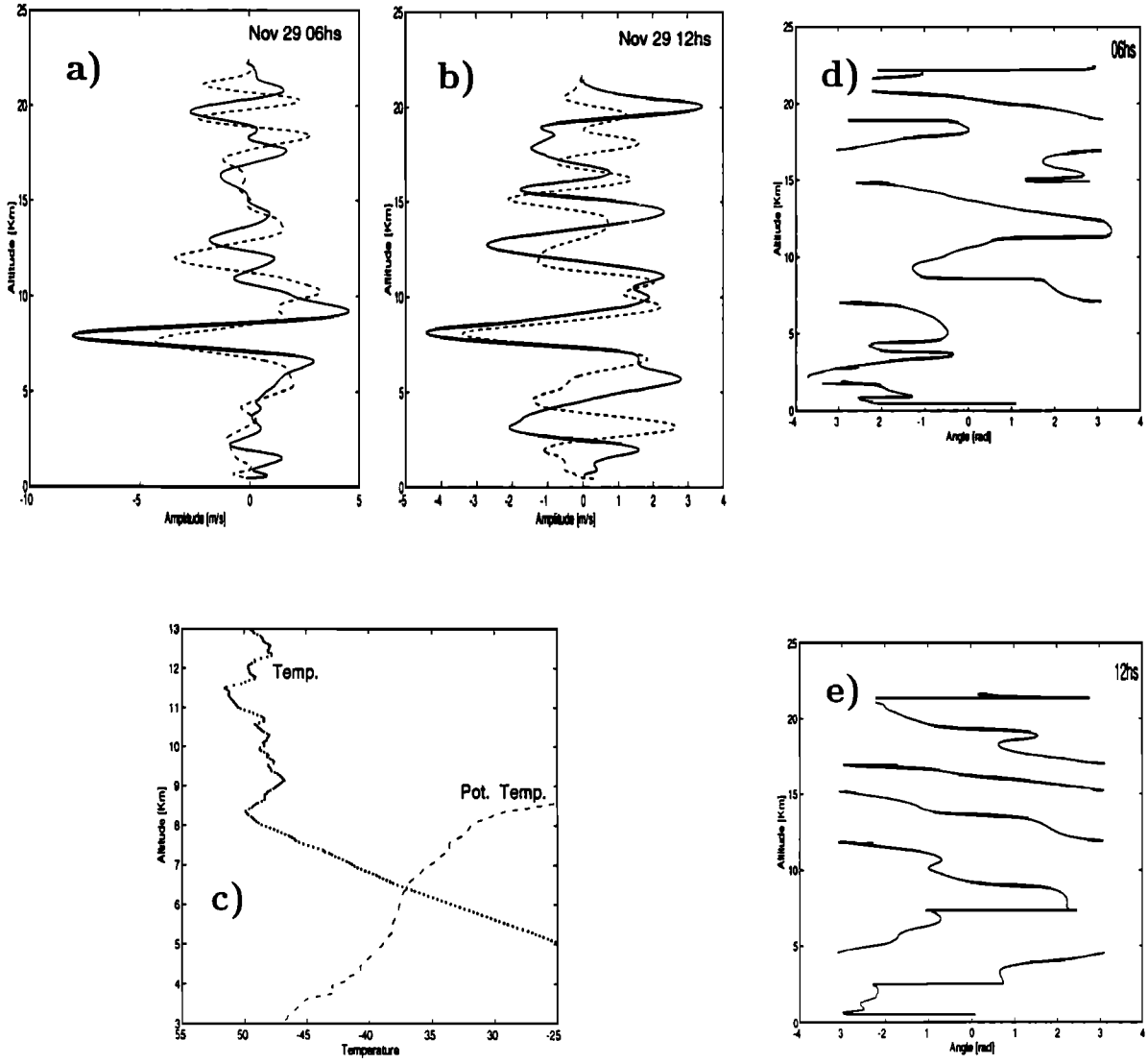

Figure 3. Pampelone soundings, November 29, 1990. (a-b) Filtered winds: zonal wind (solid); meridional wind (dashed), (c) Temperature and potential temperature at 6 UT and (d-e) angle of the filtered winds.

not possible to separate quantitatively on the soundings only the transient inertio gravity waves from the main steady waves. For this reason again, the analysis presented is only qualitative: it does not allow to conclude that the large inertio gravity waves observed near the ridge were only related to the presence of the mountain.

Example of the difference between upstream and downstream soundings is illustrated in the last two cases treated below. First, Figure 5 displays the crude data and the perturbation of the wind vector observed on November 29 at 12 UT. The dominant winds being oriented toward the south west, the downstream sounding is the one launched from Pampelone (Figures 5a-5b), the upstream sounding is the one launched from Pau (Figures 5c-5d). Downstream, one sees a mountain wave around 8 km and above, a strong inertio gravity-wave propagating upward. The upstream sounding shows rather similar patterns, the inertio-gravity wave being nevertheless smaller. In this case the fact that upstream and downstream soundings look very similar simply follows that during its ascent, the upstream balloon has been transported over the ridge by the large-scale flow. The situation is rather different on Figure 6 which shows the crude data and the perturbation of the wind vector on October 13 at 0 UT. In this case, the large-scale flow being oriented toward the north east, the upstream sounding is the one launched from Pampelone (Figures 6a-6b) and the downstream sounding is the one launched from Pau (Figures 6c-6d). Here the downstream sounding shows again a steady mountain wave just above 10 km, it is absent from the upstream sounding, the large-scale wind being too slow to transport the balloon over the ridge. It is nevertheless important to note that the upstream sounding still shows rather strong long waves. Although these waves can be due to the presence of the ridge, it can not be excluded

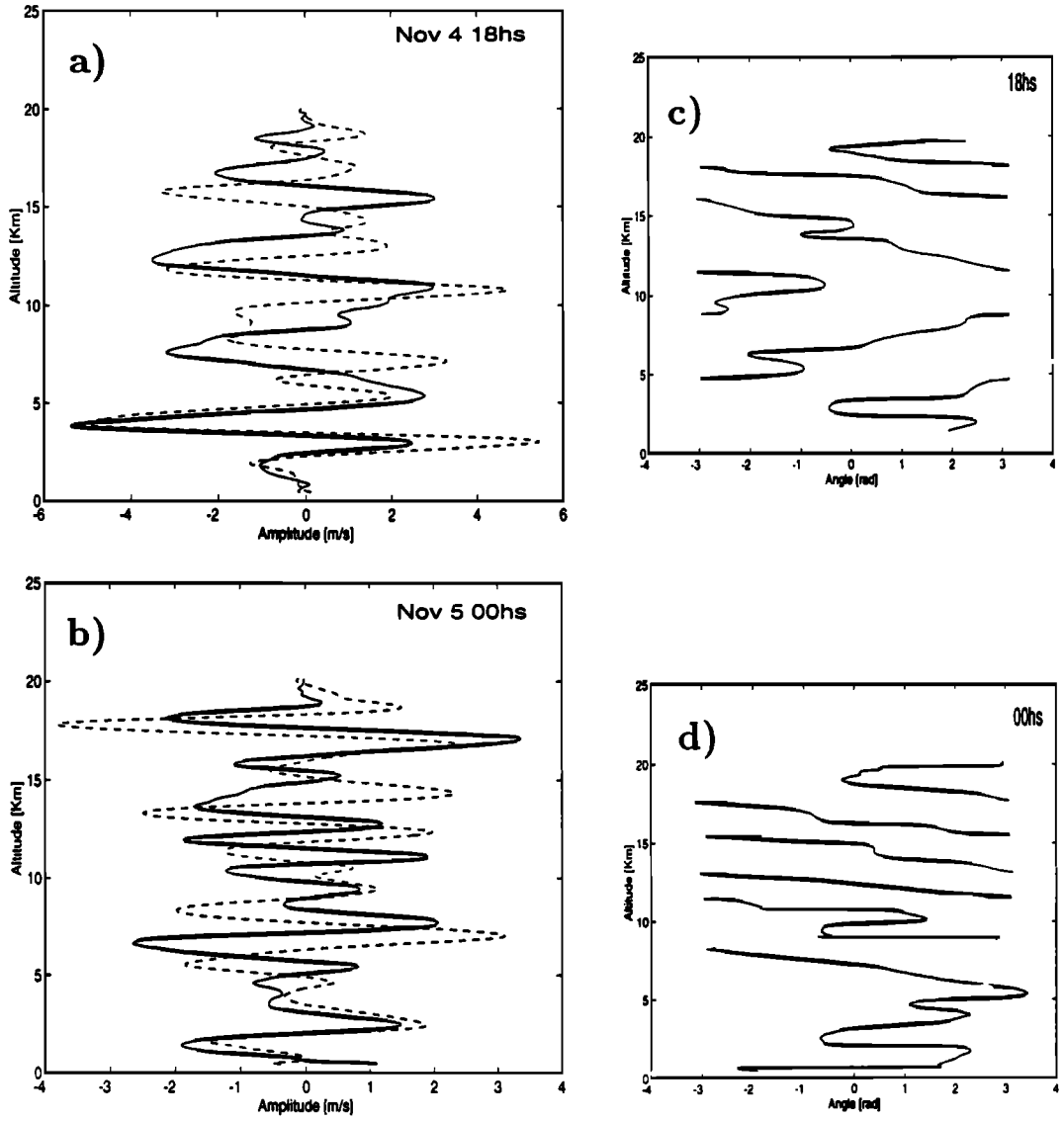

Figure 4. Pampelone soundings, November 4-5, 1990. (a)-(b) Filtered winds; zonal wind (solid) and meridional wind (dashed) and (c)-(d) angle of filtered winds.

that they are generated by other processes (geostrophic adjustment in the fronts passing close to the mountain for instance) and that they are just propagating over the Pyrénées area.

3. Theory

To analyze the waves that can follow a rather fast local momentum forcing, a simple two-dimensional model has been developed. It follows that proposed by [*Fritts and Luo*, 1992] with the important difference that the forcing used is not a dirac function in time. Its variation in time is similar to that of the measured pressure drag and its amplitude is a fraction of that drag. By making the Boussinesq and the hydrostatic approximations, assuming that the Coriolis parameter is constant, and that the forcing is essentially oriented in the meridional direction (i.e., close to that of the PYREX transect), the wave fields satisfy the equations

$$\frac{\partial u}{\partial t} - fv = 0 \tag{1}$$

$$\frac{\partial v}{\partial t} + \frac{1}{\rho_r}\frac{\partial p}{\partial y} + fu = F_y a(t) \tag{2}$$

$$\frac{1}{\rho_r}\frac{\partial p}{\partial z} - \frac{g\theta}{\theta_0} = 0 \tag{3}$$

$$\frac{\partial v}{\partial y} + \frac{\partial w}{\partial z} = 0 \tag{4}$$

$$\frac{\partial \theta}{\partial t} + \frac{\theta_0}{g}N^2 w = 0 \tag{5}$$

where u, v and w are the zonal, meridional and vertical components of the wind, θ is the perturbation potential temperature with reference to the mean value θ_0, $N^2 = (g/\theta_0)d\theta_0/dz$ is the buoyancy frequency and

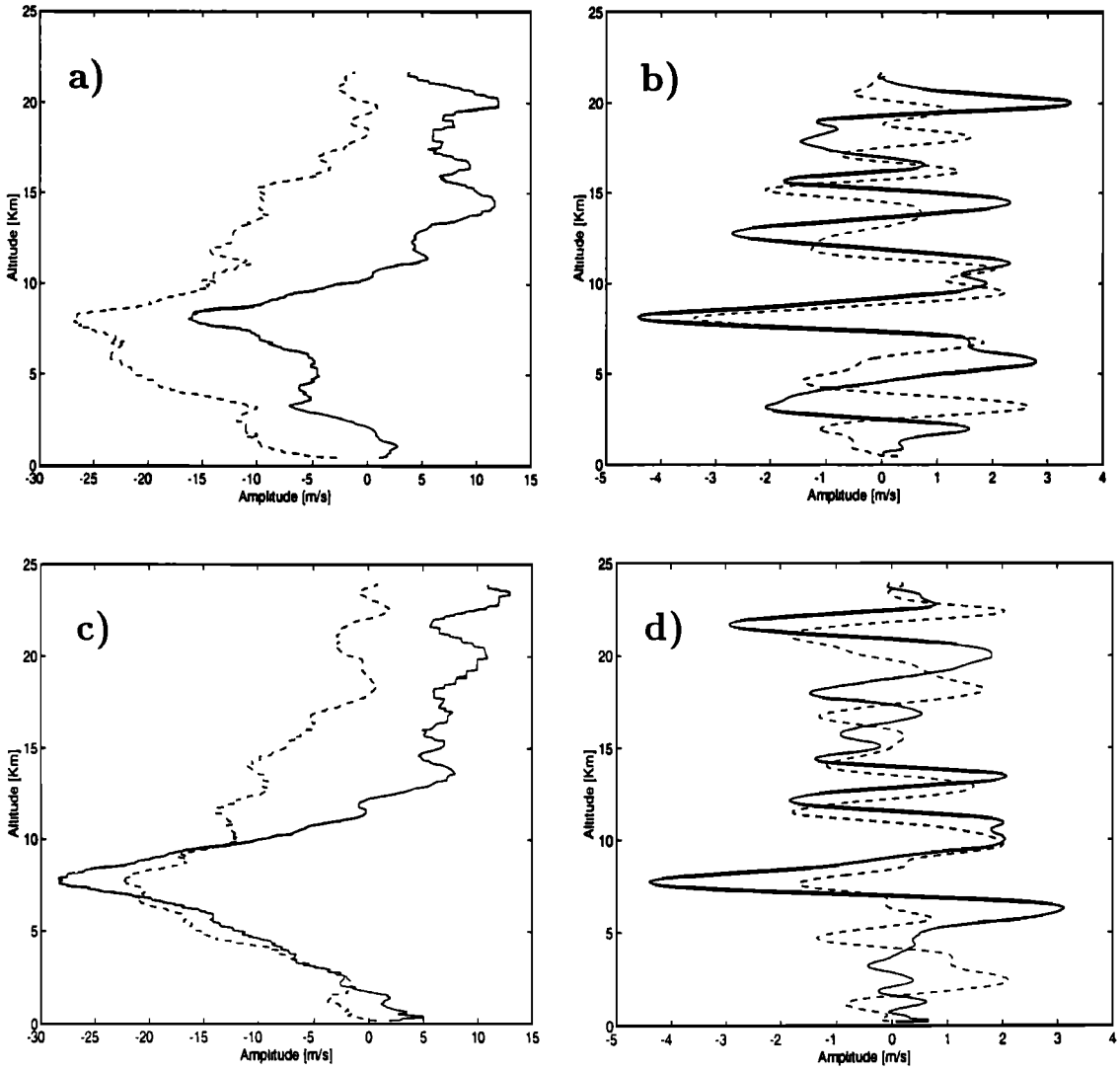

Figure 5. (a,b) Pampelone and (c,d) Pau Soundings of the horizontal wind, November 29, 1990 at 12 UT, zonal component solid and meridional component dashed. Crude data shown in Figures 5(a) and 5(c); perturbations shown on Figures 5(b) and 5(d).

ρ_r is a constant reference density. F_y and $a(t)$ represents the large-scale flow momentum forcing, due to the "breaking" main mountain waves, respectively. It is furthermore important to note that advection by the mean flow has been neglected for simplicity. On the one hand, this is justified by the qualitative character of this discussion. On the other hand, on October 26, this seems justified, the meridional wind (Figure 2) being essentially constant with altitude. Equations (1-5) can then be reduced to a set of two equations for the zonal wind u and the meridional wind v:

$$\left[\left(\frac{\partial^2}{\partial t^2}+f^2\right)\frac{\partial^2}{\partial z^2}+N^2\frac{\partial^2}{\partial y^2}\right]u = f\frac{\partial^2}{\partial z^2}\left[F_y a(t)\right] \quad (6)$$

$$\left[\left(\frac{\partial^2}{\partial t^2}+f^2\right)\frac{\partial^2}{\partial z^2}+N^2\frac{\partial^2}{\partial y^2}\right]v = \frac{\partial^2}{\partial z^2}\left[F_y\frac{da(t)}{dt}\right] \quad (7)$$

These equations can be solved in the spectral space, considering that the wave field is made of a superposition of harmonics,

$$u = \int_{-\infty}^{+\infty} \Re\left\{\tilde{u}\exp^{i(ly+mz)}\right\} dldm \ , \quad (8)$$

with meridional and vertical wavelength, l and m. Then, for each harmonic, (6) and (7) become

$$\tilde{u}'' + \omega^2\tilde{u} = f\tilde{F}_y a(t) \ ; \ \tilde{v}'' + \omega^2\tilde{v} = \tilde{F}_y a'(t). \quad (9)$$

where $\omega^2 = f^2 + N^2l^2/m^2$. Then, solving the two equations,

$$\psi_1'' + \omega^2\psi_1 = a(t) \quad \psi_2'' + \omega^2\psi_2 = a'(t) \quad (10)$$

the solution writes

$$\tilde{u} = f\tilde{F}_y\psi_1(t) \quad \tilde{v} = \tilde{F}_y\psi_2(t). \quad (11)$$

To put a momentum forcing that is coherent in time with the fluctuations of the drag measured at the ground,

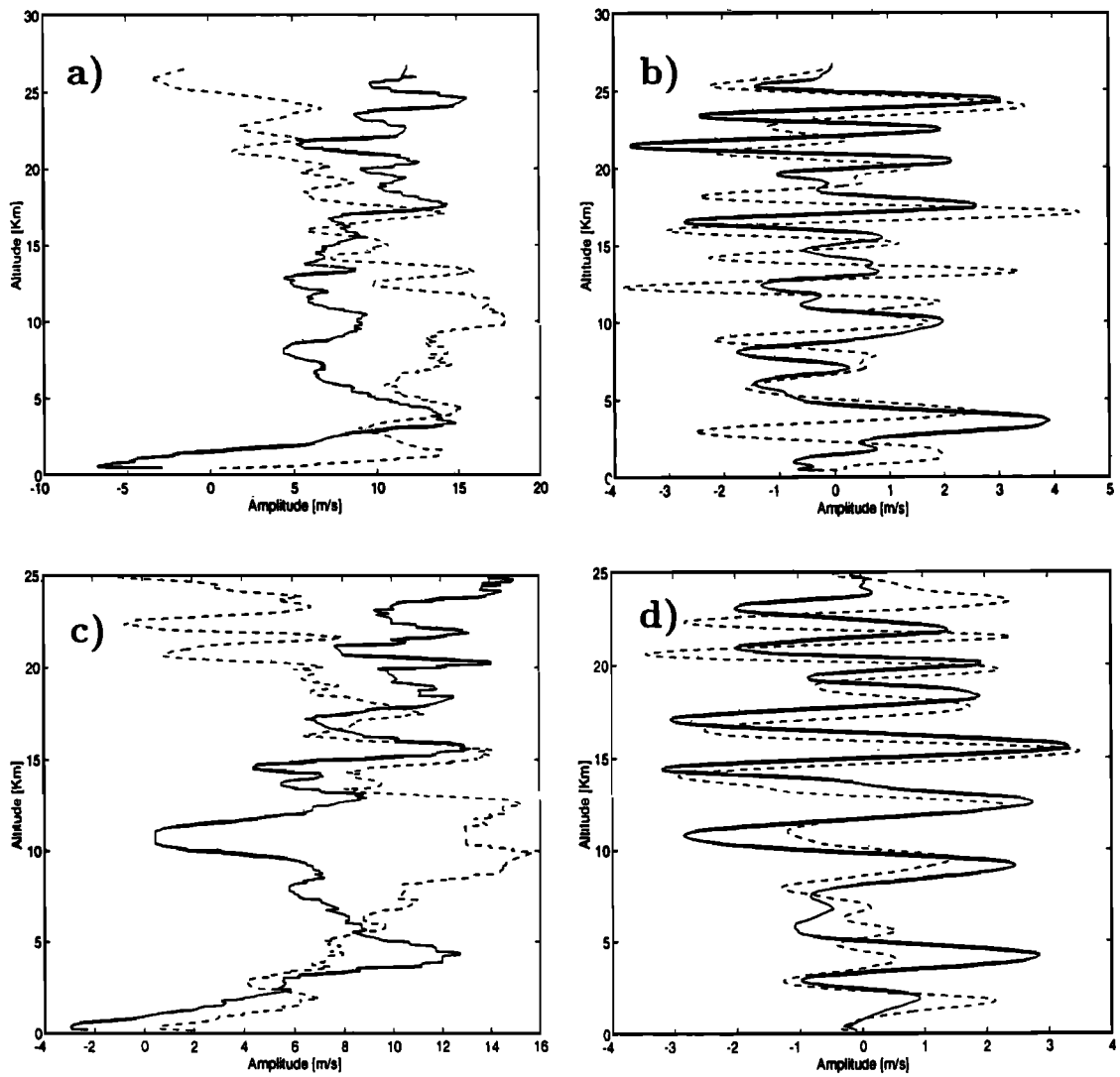

Figure 6. (a,b) Pampelone and (c,d) Pau Soundings of the horizontal wind, October 13, 1990 at 0 UT, zonal component solid and meridional component dashed. Crude data shown in Figures 6(a) and 6(c); perturbations shown on Figures 6(b) and 6(d).

the amplitude of the momentum source starts from zero, reaches a positive value in 10 hours, and returns to 0 in 10 hours. This forcing mimics the rapid and strong peak of negative mountain drag that lasts less than a day between October 35 and 26, and goes down to nearly -6 Pa:

$$\begin{aligned} a(t) &= \sin \lambda t \quad \text{if } t < \pi/\lambda \\ a(t) &= 0 \quad \text{if } \pi/\lambda < t \end{aligned} \tag{12}$$

and $\pi/\lambda = 20$ hours. Then, the solutions of (11) with zero initial value are

$$\begin{aligned} \psi_1 &= \frac{\omega \sin \lambda t - \lambda \sin \omega t}{\omega(\omega^2-\lambda^2)} \quad \text{if } t < \frac{\pi}{\lambda} \\ \psi_1 &= \frac{\lambda(\sin \omega(\frac{\pi}{\lambda}-t) - \sin \omega t)}{\omega(\omega^2-\lambda^2)} \quad \text{if } \frac{\pi}{\lambda} < t \end{aligned} \tag{13}$$

$$\begin{aligned} \psi_2 &= \frac{\lambda(\cos \lambda t - \cos \omega t)}{\omega^2-\lambda^2} \quad \text{if } t < \frac{\pi}{\lambda} \\ \psi_2 &= -\frac{\lambda(\cos \omega t + \cos \omega(t-\frac{\pi}{\lambda}))}{\omega^2-\lambda^2} \quad \text{if } \frac{\pi}{\lambda} < t \end{aligned} \tag{14}$$

Then, it is further assumed that the spatial form of the forcing is given by

$$F_y = A \exp\left(-\frac{y^2}{2{\sigma_y}^2} - \frac{z^2}{2{\sigma_z}^2}\right) \cos K_z z \tag{15}$$

with $\sigma_y = 50$ km, $\sigma_z = 2$ km and $2\pi/K_z = 6$ km. The value of σ_z was chosen to represent the neutrally buoyant 2 km layer observed at 0 TU October 26. The cosinus function in the vertical direction is introduced to make sure that the forcing becomes zero at a finite distance of its maximum, as should occur if the main waves break in a layer which depth does not exceed a certain fraction of the primary waves vertical wavelength. The change of sign below and above $Z = 3$ km is quite unrealistic, but the results obtained were not found to be very sensitive to this parameter, providing it remains above $K_z > 2\pi/(10\text{ km})$. The choice of σ_y was made to render the forcing area length, com-

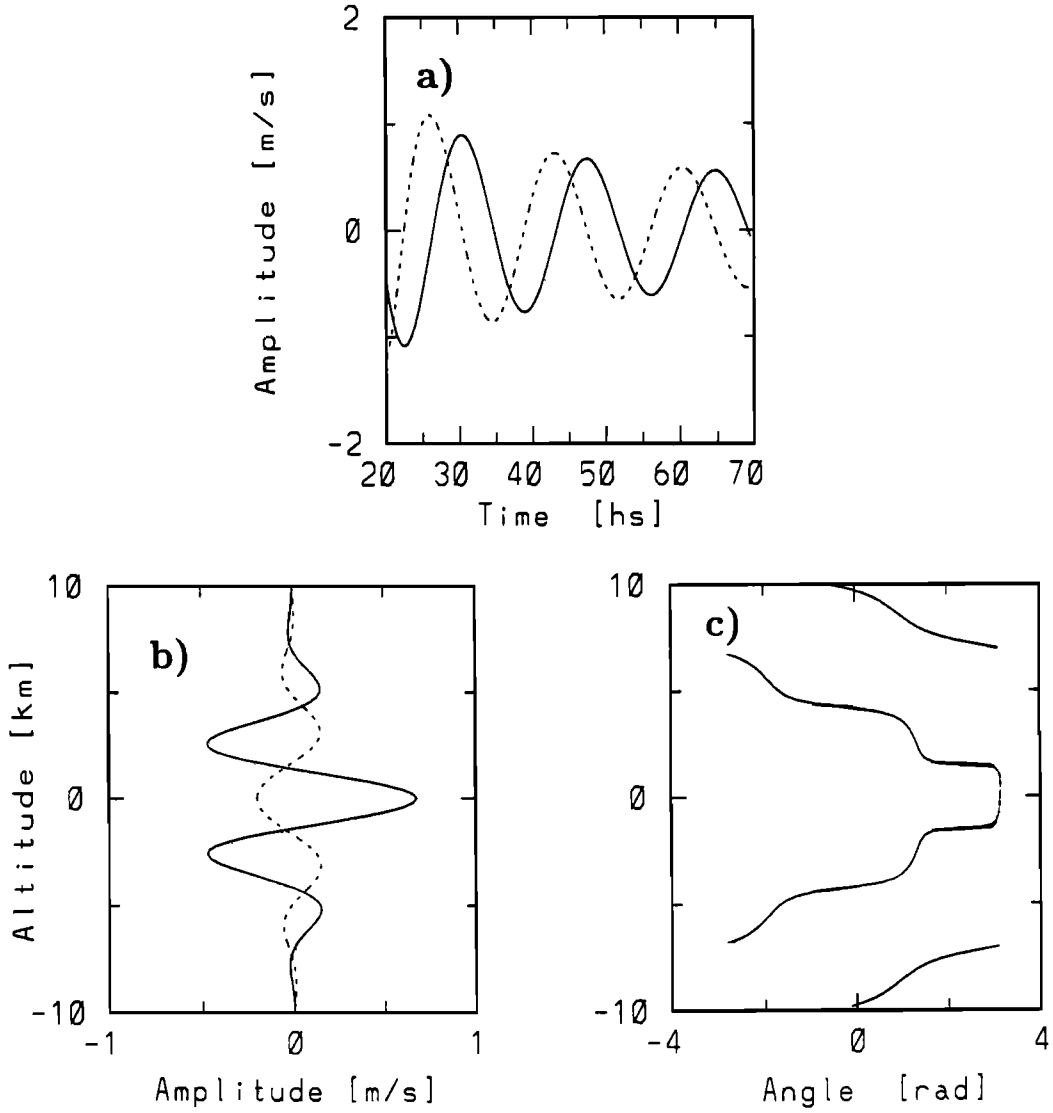

Figure 7. Analytical results (see text for details). (a) Temporal evolution of the zonal (solid) and meridional (dashed) winds at $z = 0$ and $y = 0$, (b) vertical section of the zonal (solid) and meridional (dashed) winds at y=150 km and t=32 hours (12 hours after the end of the forcing). (c) Angle of the winds.

parable to the Pyrénées length. This further assumes that orographic wave breaking and turbulence can occur nearly everywhere above the massive. The amplitude, $A = 7\,10^{-4}\,\mathrm{m\,s^{-2}}$, is chosen so that at its maximum the overall momentum forcing, expressed in Pascals,

$$\frac{1}{2\sigma_y}\int_{-\infty}^{+\infty}\int_{-\infty}^{+\infty}\rho_r F_y(y,z)dydz \approx 1\,\mathrm{Pa} \qquad (16)$$

is more than 5 times smaller than the measured pressure drag. This is well in agreement with the fact that in the atmosphere the momentum fluxes transported by the vertically propagating mountain waves are typically 1 order of magnitude smaller than the mountain drag [*Bougeault et al.*, 1993]. It also assumes that only part of the momentum is restored to the mean flow at the location where the waves break. Then, calculating the Fourier transform of the forcing equation (16), the horizontal wind perturbation fields can be evaluated using (11). The solutions u and v as a function of the time are presented in Figure 7a. The values $N = 10^{-2}\,\mathrm{s^{-1}}$ (typical of that observed during the PYREX campaign) and $f = 10^{-4}\,\mathrm{s^{-1}}$ have also been adopted.

Figure 7 shows features which have many points in common with the observations. After the maximum of the forcing, inertial waves radiate from the forcing area, the phase rotation being cyclonic when the altitude increases above that level and anticyclonic below. The amplitude of these waves is of the order of the meters per second which is also the order of magnitude of the inertial waves that were observed in the soundings. Sensitivity experiments to the different parameters, σ_y, σ_z and K_z has been done. For significant waves to be emitted in a fraction of time that is compatible

with the observations (i.e., 6 hours), and to give rise to rather well-defined inertio-gravity waves, it appears that the parameter σ_z should not exceed few kilometers. Sensitivity experiments to the parameter σ_y indicate that significant well-defined inertio-gravity waves can appear, providing that 50 km $< \sigma_y$. This means that the mechanisms proposed here are only relevant if one can consider that the waves forced by the ridge act on the large-scale flow over a distance that compare to the ridge depth.

4. Conclusions

The analysis of high-resolution soundings have allowed us to describe different type of waves observed in the lee of the Pyrénées during the PYREX campaign. In agreement with other observations made during the campaign, those soundings often show coherent high intrinsic frequency gravity waves, which are directly forced by the mountain. Nevertheless, those soundings more systematically show very coherent inertio-gravity waves of large amplitude. Although those waves can be related to processes that are not directly linked to the presence of the ridge (geostrophic adjustment in the fronts passing close to the mountain for instance), there are some observational indications that those waves can be partly attributed to the presence of the mountain. Indeed, it appears rather frequently that the observed inertio-gravity waves are propagating away from levels where the main mountain waves were very large some time before and eventually close from breaking. Nevertheless, the low density of the soundings network does not allow us to conclude definitely on this last issue. Furthermore, the observation of adiabatic lapse rates in individual soundings is not a definitive proof that breaking occurs. For these reasons, the analysis presented is just qualitative. It should nevertheless be kept in mind that wave breaking is not the only configuration for which waves can interact with the large-scale flow [*Grimshaw,* 1975; *Andrews and McIntyre,* 1976], and the fact that the main mountain waves amplitude varies in time without breaking can also lead to a large-scale transient forcing which can also give rise to inertio-gravity waves.

Then, to test if some inertio-gravity waves can result from an indirect forcing due to the ridge, a simple model of inerto-gravity waves forced by a transient momentum deposition has been developed. This model is very simple and only provides a scale analysis of the inertio-gravity waves amplitude that can be expected from the mountain forcing. This model nevertheless shows that when a momentum deposit which amplitude is significantly smaller than the measured mountain drag and that occurs during a short finite time (less than a day), inertio-gravity waves with amplitude comparable to those observed in the soundings can be found. In this simple mechanistic model the hypothesis that the momentum forcing is smaller than the drag measured at the ground is justified by the fact that in the observations the main mountain waves only transport a fraction of the mountain drag (see, for instance, the momentum flux profiles and the pressure drag records of [*Bougeault et al.,* 1993]). The fact that the forcing is very transient is consistent with the observation of rapid (less than a day) changes in the pressure drag. Nevertheless, it should also be kept in mind that the model we have used overstates the possibility of wave emission from a given forcing. Indeed, a significant part of the momentum given to the flow will result in balanced large-scale features instead of forcing inertio-gravity waves.

Appendix

The filtering process used consists in extracting the waves in the range 2 to 6 km by applying first a low-pass filter that suppresses the wavelength smaller than 2 km. On the resulting data is applied a low-pass filter that suppresses the wavelength lower than 6 km. The waves are obtained as the difference between the results of the two preceding filtered samples. In essence, the filter used being non recursive, it can be written

$$\tilde{y}(n) = \sum_{p=-N}^{p=+N} a(p)y(n-p) \quad , \text{ for } N < n < P - N$$

where $a(n)$ are the coefficients of the filter: they satisfy $\sum_{-N}^{+N} a(p) = 1$ and $a(-p) = a(p)$. This last symmetry property is important: it implies that the filter does not affect the phase of the signal harmonics. The order of the filter and the number of data in the initial samples are $N = 100$ and $M = 600$ typically (note nevertheless that M varies significantly from one soundings from the other, depending on the altitude reached). Furthermore, to avoid Gibbs phenomenon, the coefficients of the filter correspond to a low-pass filter with Kayser window [*Hamming,* 1983]. In general, the larger the order N is, the sharper is its response around the cutoff frequency, and the value $N = 100$ has been adopted. Nevertheless, near the upper and lower bounds of the sample the order of the filter decreases in order that only data located inside the soundings are considered (there is no need to extrapolate and enlarge them artificially). In this case the filter coefficients were kept unchanged, but the order varies from one point to another. It is $n - 1$ near the lower bound and $M - n - 1$ near the upper bound. In these cases, since the sums $\sum_{-n+1}^{n-1} a(p) < 1$ or $\sum_{-M+n+1}^{M-n-1} a(p) < 1$, the filter coefficients are divided by these sums. The behavior of the filter for various values of the order is illustrated in Figure 8a that shows the transfer function

$$T_N(\lambda) = \sum_{-N}^{+N} a(p) e^{i(2\pi\lambda p \delta z)} .$$

The fact that the transfer function depends on the filter

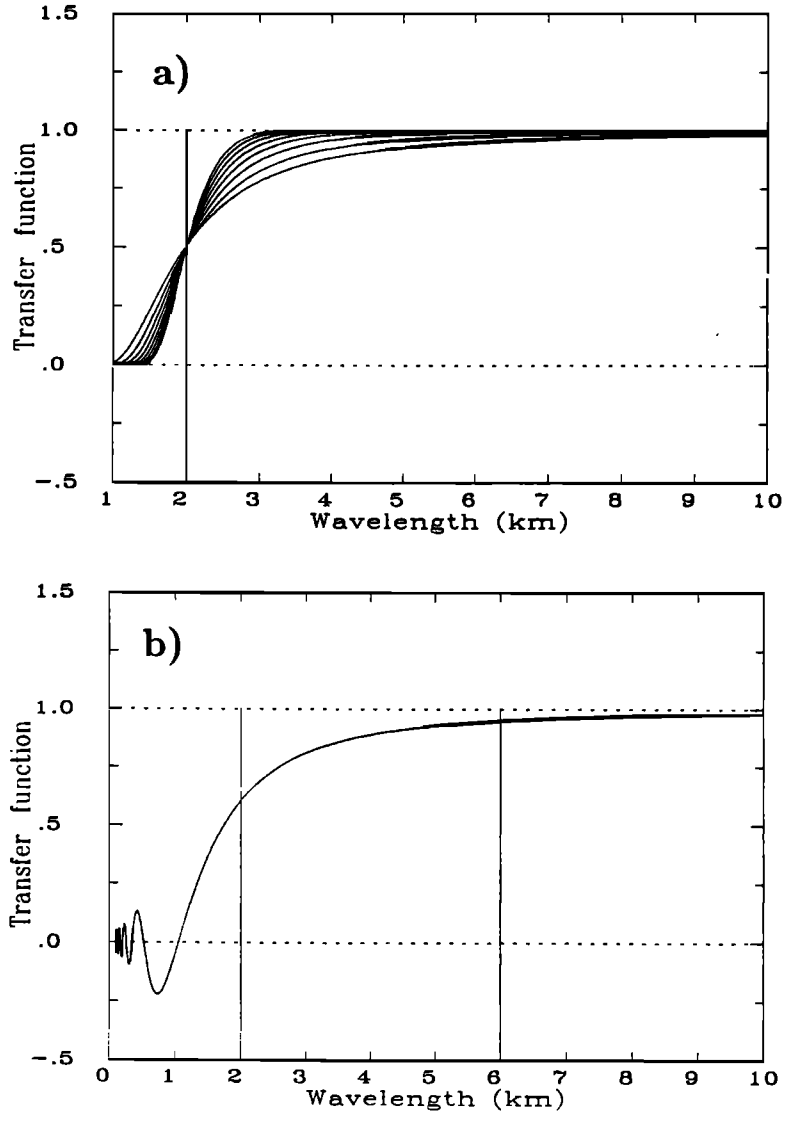

Figure 8. Transfer function of the various filters used in the study. (a) The 2 km low-pass filter for N=40,...,110 and (b) the moving average of buffer length 1200 km.

order, make that near the bounds, it is different from one altitude to another. Nevertheless, and as verified in Figure 8a, it is shown that the filter converges quite rapidly when N increases. It is also important to note that for all values of the order N, the cutoff frequency 2 km, in Figure 8a.) is always properly located. Nevertheless, near the bounds (i.e., for $N < 40$) the transition between filtered and unfiltered wavelength is no longer sharp, and the filter affects significantly the amplitude of the harmonics up to 6 km. It means that all the waves will be reduced at distances less than 2 km from the bound. As the same remarks are true for the 6 km low-pass filter used, the preceding remarks show that the filter will affect the waves at less then 6 km from the bounds. Nevertheless, as the filters are totally free of Gibbs effects, the resulting data will never overstate the wave signal: they are free of spurious waves.

Furthermore, it is noteworthy that contrary to the thermodynamics variables, spanned every 50 m, the wind profiles are filtered initially. This results from a smoothing applied routinely to suppress the noise due to the inaccuracy of the positionning of the balloons by the Loran-C (or the Omega) system used. This operational smoothing is a kind of moving average which buffers length varies with altitude. During PYREX it was below 1200 m (P. Bessemoulin, private communication, 1997). The transfer function of such a filter applied to data like those used in this study is displayed in Figure8b. It shows that the moving average eventually introduces spurious ripples but at scales significantly below 2 km. Those ripples are then removed by the 2 km low-pass filter described above. It is also noteworthy that the moving averaged is not a sharp filter: it decreases quite significantly all the wavelength

below 6 km. The moving average being symmetrical in essence, it will not affect the phase of the extracted harmonics.

To summarize, it appears that the different filters significantly reduce the amplitude of the harmonics extracted. This defect is a consequence of the fact that we have tried to get rid of all Gibbs effects and from the fact that the soundings have finite length. The filters used have the important property that they preserve the phase of the harmonics. As a consequence, the waves analyzed in the paper never overstate the real disturbances amplitude in the 2-6 km range, and the information on the phase is always robust.

References

Andrews, D. G., and M. E. McIntyre, Planetary waves in horizontal and vertical shear: the generalized Eliassen Palm relation and the mean zonal acceleration, *J. Atmos. Sci.*, *33*, 2031-2048, 1976.

Bessemoulin, P., P. Bougeault, A. Genoves, A. Jansa Clar, and D. Puech, Mountain pressure drag during PYREX, *Beitr. Phys. Amos.*, *4*, 305-325, 1993.

Blumen, W., Geostrophic adjustment, *Rev. Geophys.*, *10*, 485–528, 1972.

Bougeault, P., et al., The atmospheric momentum budget over a major mountain range: first results of the PYREX field program, *Ann. Geophys.*, *11*, 395-418, 1993.

Bretherton, C. S., and P. K. Smolarkiewitcz, Gravity waves, compensating subsidence and detrainment around cumulus clouds, *J. Atmos. Sci.*, *46*, 740-759, 1989.

Champeaux, J. L., and P. Peris, Atlas des données sol de Météo-France pendant l'expérience PYREX, *Notes de Centre 3, Cent. Natl. Rech. Meteorol., F31057 Toulouse, France*, 1991.

Fritts, D. C., Shear excitation of atmospheric gravity waves, *J. Atmos. Sci.*, *39*, 1936-1952, 1982.

Fritts, D. C., and Z. Luo, Gravity wave excitation by geostrophic adjustment of the jet stream, *J. Atmos. Sci. 49*, 681-697, 1992.

Georgelin, M., E. Richard, M. Petitdidier, and A. Druilhet, Impact of subgrid-scale orography parameterization on the simulation of orographic flows, *Mon. Weather Rev., 122*, 1509-1522, 1994.

Grimshaw, R., Nonlinear internal gravity waves and their interaction with the mean wind, *J. Atmos. Sci.*, *32*, 1779–1793, 1975.

Hamming, R. W., *Digital Filters*, Englewood Cliffs: Prentice-Hall, 1983.

Lalas, D. P., and F. Einaudi, On the characteristics of gravity waves generated by atmospheric shear layers, *J. Atmos. Sci.*, *33*, 1248-1259, 1976.

Lott, F., and H. Teitelbaum, Linear unsteady mountain waves, *Tellus Ser. A*, *45*, 201-220, 1993.

Lott, F., H. Kelder, and H. Teitelbaum, A transition from Kelvin-Helmholtz instabilities to propagating wave instabilities, *Phys. Fluids A*, *9*, 1990-1997, 1992.

Mattocks, C., and R. Bleck, Jet streak dynamics and geostrophic adjustment processes during the initial stages of lee cyclogenesis, *J. Atmos. Sci., 114*, 2033-2056, 1986.

Palmer, T. N., G. J. Shutts, and R. Swinbank, Alleviation of systematic westerly bias in general circulation and numerical weather prediction models through an orographic gravity wave drag parametrization, *Q. J. R. Meteorol. Soc.*, *112*, 2056-2066, 1986.

Queney, P., *Theory of perturbations in stratified currents with application to airflow over mountains, Misc. 23*, Univ. of Chicago Press, 1947.

Rosenthal, A. J., and R. S. Lindzen, Instabilities in a stratified fluid having one critical level. Part 2: Explanation of gravity wave instabilities using the concept of overreflection, *J. Atmos. Sci.*, *40*, 521-529, 1983.

Rossby, C. G., On the mutual adjustment of pressure and velocity distributions in certain simple current systems, *J. Mar. Res.*, *21*, 15-28, 1937.

Schär, C., and D. R. Durran. Vortex formation and vortex shedding in continuously stratified flows past isolated topography, *J. Atmos. Sci.*, *54*, 534-554, 1996.

Shutts, G. J., and M. E. B. Gray, A numerical modelling of the geostrophic adjustment process following deep convection, *Q. J. R. Meteorol. Soc.*, *120*, 1145-1178, 1994.

Smith, R. B., The influence of mountains on the atmosphere, *Adv. Geophys.*, *21*, 87-230, 1979.

M. A. Lamfri and C. M. Scavuzzo, Faculdad de Matematica, Astronomia y Fisica, Universidad Nacional de Cordoba, Ciudad Universitaria, Cordoba 5000, Argentina. (e-mail: scavuzzo@roble.fis.uncor.edu; lamfri@roble.fis.uncor.edu)

F. Lott and H. Teitelbaum, Laboratoire de Météorologie Dynamique, Ecole Normale Supérieure, 24 rue Lhomond, 75231 Paris Cédex 05, France. (e-mail:teitel@lmd.ens.fr; flott@lmd.jussieu.fr)

(Received February 17, 1997; revised July 18, 1997; accepted August 6, 1997.)